Accelerated Publications

Trapping of the S_2 to S_3 State Intermediate of the Oxygen-Evolving Complex of Photosystem II†

Nikolaos Ioannidis, Georgia Zahariou, and Vasili Petrouleas*

Institute of Materials Science, NCSR "Demokritos", 153 10 Aghia Paraskevi Attikis, Greece

Received March 15, 2006; Revised Manuscript Received April 18, 2006

ABSTRACT: Photosystem II preparations poised in the $S_2\cdots Q_A$ state produce no detectable intermediate during straightforward illumination at liquid helium temperatures. However, upon flash illumination in the range of 77−190 K, they produce a transient state which at −10 °C advances to S_3 or after rapid cooling to 10 K gives rise to a 116 G wide metalloradical EPR signal. The latter decays with half-times on the order of a few minutes, presumably by charge recombination, and can be regenerated repeatedly by illumination at 10 K. The constraints for Tyr Z oxidation are attributed to the presence of excess positive charge in S_2. Elevated temperatures are required presumably to overcome a thermal barrier in the deprotonation of Tyr Z^+ or most likely to allow secondary proton transfer away from the base partner of Tyr Z. Treatment with 5% (v/v) MeOH appears to remove the constraints for Tyr Z oxidation, and a 160 G wide metalloradical EPR signal is produced by illumination at 10 K, which decays with a half-time of ca. 80 s. Formation of the metalloradical signals is accompanied by reversible changes in the Mn multiline signal. The intermediates are assigned to Tyr $Z^\bullet$ magnetically interacting with the Mn cluster in S_2, $S_2Y_Z^\bullet$. A molecular model which extends an earlier suggestion and provides a plausible explanation of a number of observations, including the binding of small molecules to the Mn cluster, is presented.

The oxygen-evolving complex of photosystem II undergoes periodically four one-electron oxidation steps, S_0 to S_1, ..., S_3 to $(S_4)S_0$, driven by the photooxidizable chlorophyll species P_{680}.[1] The oxidizing equivalents are stored at or in the immediate vicinity of a Mn cluster (the site of water oxidation, believed to be tetranuclear). Electron transfer between P_{680}^+ and the Mn cluster is mediated by tyrosine Z, Tyr Z or Y_Z. Oxygen evolves during the $S_3-(S_4)S_0$ transition, S_4 being a transient state (*1*, *2*).

The S state transitions have an unusual temperature dependence pattern (*3*, *4*). Three of the transitions, from S_0 to S_1, from S_2 to S_3, and from S_3 to S_0, have half-inhibition temperatures of ∼230 K (220−225, 230, and 235 K, respectively, for the three transitions), while the S_1 to S_2 transition has a much lower inhibition temperature. This transition can be induced at 77 K at least in part (ref *5* and our unpublished results). There are two major sequential steps on each S state transition: oxidation of Tyr Z by P_{680}^+ to the neutral radical form, Tyr $Z^\bullet$, and oxidation of the Mn cluster by Tyr $Z^\bullet$. The blockage of the S state transitions below certain temperatures could in principle be due to blockage of either of the steps mentioned above or both. Accumulating evidence in recent years suggests that Tyr Z can be oxidized at liquid helium temperatures as an intermediate of certain but not all S state transitions. These intermediates, detected by EPR spectroscopy, have the characteristics of a radical magnetically interacting with a paramagnetic metal species and have been tentatively assigned to Tyr $Z^\bullet$ magnetically interacting with the Mn cluster in its various oxidation states (*5*−*10*). Curiously, Tyr Z can be directly oxidized by P_{680}^+ at liquid helium temperatures in the S_0 and S_1 states but not in the higher S_2 and S_3 states. This has been correlated with the fact that the OEC is more positively charged in the latter two states (*10*). Since thermodynamic restrictions impose deprotonation of Tyr Z during its oxidation by P_{680}^+ (*11*), the blockage of Tyr Z oxidation in the S_2 and S_3 states has been attributed formally to a lowering of the p*K* of the base partner of Tyr Z, base B (presumably His 190 of the D1 polypeptide), by the more positive charge on the Mn cluster (*10*). This interpretation is supported among other things by the observation that one-electron reduction of the Mn cluster in the S_3 state at 77 K (a temperature at which proton uptake from the aqueous phase is inhibited) creates a less positively charged S_2

† Financial support of the AKMWN program of the Greek GSRT is kindly acknowledged.

* To whom correspondence should be addressed. Telephone: +301 650-3344. Fax: +301 651-9430. E-mail: vpetr@ims.demokritos.gr.

[1] Abbreviations: PSII, photosystem II; OEC, oxygen-evolving complex; S states, S_0-S_4 oxidation states of the OEC; Tyr Z or Y_Z, tyrosine 161 of the D2 protein; tyrD or Y_D, tyrosine 160 of the D1 protein; P_{680}, primary electron donor in PSII; signal II, EPR signal of either of the two isolated tyrosine radicals; metalloradical or split signals, EPR signals in the $g = 2$ region attributed to the broadening of the Tyr $Z^\bullet$ spectrum by a weak magnetic interaction with the Mn cluster; Q_A and Q_B, primary and secondary plastoquinone electron acceptors of PSII, respectively; MES, 2-(*N*-morpholine)ethanesulfonic acid; chl, chlorophyll; duroquinone, tetramethyl-*p*-benzoquinone; NIR, near-infrared; EPR, electron paramagnetic resonance.

10.1021/bi060520s CCC: $33.50
Published on Web 05/03/2006

configuration, S_2'; Tyr Z is readily oxidized in the S_2' configuration by visible light illumination at 4.2 K, producing the intermediate $S_2'Y_Z^\bullet$ (*9*). These observations imply a special arrangement of Tyr Z, base B, and the Mn cluster (*10*) and in combination with the recent important advances in the X-ray elucidation of the OEC structure (*12*−*14*) open new prospects to understanding of important mechanistic details of the water-splitting reaction.

The S_2 to S_3 step has been the subject of extensive experimentation. The S_3 state converts to what appears to be an $S_2Y_Z^\bullet$ intermediate at alkaline pH (*15*), while early inhibitory treatments of the OEC (Ca^{2+} depletion or acetate treatment) yielded nonfunctional (unable to advance to the S_3 state) intermediates (*16*, *17*) attributed by most authors to $S_2Y_Z^\bullet$ (refs *18*−*20*, but see ref *21*). The latter intermediates could be produced only at temperatures close to 250 K and above and were stable at cryogenic temperatures.

In this paper, we show that it is possible to trap an S_2 to S_3 state intermediate in oxygen-evolving PSII preparations. Illumination at temperatures in the range of 77−190 K produces a transient state that can either advance to the S_3 state when it is rapidly heated to −10 °C or yield a transient 116 G broad metalloradical EPR signal when it is quickly cooled to 10 K. After its decay at 10 K (presumably by charge recombination), the signal can be repeatedly re-formed by illumination at 10 K and can advance to the S_3 state when it is rapidly heated to −10 °C. Treatment with methanol appears to remove the constraints for Tyr Z oxidation in S_2, and illumination at 10 K results in the formation of a 160 G metalloradical EPR signal. Formation of the metalloradical intermediates of the S_2 to S_3 state transition is accompanied by reversible changes in the S_2 state multiline EPR spectrum. The intermediates are assigned to $S_2Y_Z^\bullet$. A molecular model extending our earlier suggestion (*10*) is presented, which appears to explain a number of experimental observations.

MATERIALS AND METHODS

PSII Sample Isolation. PSII-enriched thylakoid membranes were isolated from spinach (procedure from ref *22* with modifications). Samples for EPR measurements were suspended in 0.4 M sucrose, 15 mM NaCl, and 40 mM MES (pH 6.5) at ∼6−8 mg of chl/mL and stored in liquid nitrogen. All samples were supplemented with 1 mM duroquinone as an exogenous electron acceptor. No iron oxidation occurs with duroquinone (*23*). Methanol was added only when specifically indicated.

Illumination Conditions. Two studio photographic power supplies were used for flash excitation of samples: a 600 W device with a pulse duration of 2.1 ms, at temperatures below ca. 220 K, and a 200 W device with a pulse duration of 1.2 ms, at temperatures above 220 K. The latter produced single turnovers at −5 °C. Continuous illumination for a few minutes at temperatures below ∼220 K produced results qualitatively similar to those of the flash excitation except that the long period of illumination interfered with the lifetime of the transient signals.

The $S_2\cdots Q_A$ state was produced by the following protocol or variants of it (replacement, for example, of the flash illumination at 190 K with continuous illumination). Samples were given single-flash illumination at −5 °C and kept at the same temperature for 30 s to allow electron transfer from Q_A to duroquinone. This produced 80% of S_2 and no detectable amount of S_3. S_2 was subsequently maximized by a strong flash at 190 K followed by a 1 min dark adaptation at the same temperature (to eliminate the small fraction of centers that would advance to S_3 as described in this paper) before being heated to −10 °C for 30 s. The $S_2\cdots Q_A^-$ state was produced by continuous illumination at 190−200 K, for 3−4 min, of samples that were previously poised in the S_1 state by single-flash illumination at −5 °C and subsequent dark adaptation at 5 °C for 30 min.

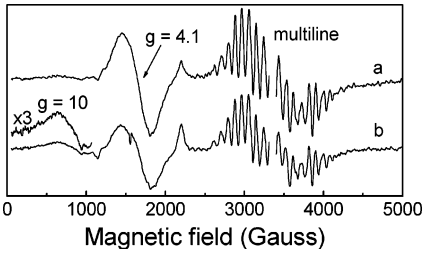

FIGURE 1: Stepwise activation of the S_2 to S_3 transition by flash illumination of S_2 at 190 K, followed by rapid heating to −10 °C. Difference spectra vs the S_1 state are shown: (a) S_2 state prepared by flash illumination of S_1 at −5 °C and (b) flash illumination of the S_2 state at 190 K followed by rapid transfer (within 1−2 s) and incubation (for 30 s) at −10 °C. This procedure was repeated 10 times. EPR conditions: microwave frequency of 9.407 GHz, temperature of 10 K, modulation amplitude of 25 G, and microwave power of 32 mW.

For the trapping of the S_2 to S_3 intermediate, untreated samples in the S_2 state were flash-excited in the range of 77−190 K (liquid nitrogen, isopentane, or acetone cooled with liquid N_2 was used as the coolant) and immediately transferred to liquid nitrogen and from there into the EPR cryostat at 10 K. To maximize the yield of the intermediate, three flashes spaced by 2 s were given in each case, resulting in a 40% increase in the yield compared to that with a single flash.

EPR Measurements. EPR measurements were obtained with an upgraded Bruker ER-200D spectrometer interfaced with a personal computer and equipped with an Oxford ESR 900 cryostat, an Anritsu MF76A frequency counter, and a Bruker 035M NMR gaussmeter. The Signal-Channel unit was replaced with an SR830 digital lock-in amplifier from Stanford Research. The perpendicular 4102ST cavity was used, and the microwave frequency was 9.41 GHz.

RESULTS

Trapping of an Intermediate of the S_2 to S_3 Transition in Untreated Samples. Whether an intermediate of the S_2 to S_3 transition can be trapped at temperatures sufficiently lower than the threshold for the S_2 to S_3 transition of 230 K was examined (*3*, *4*). Figure 1a shows the spectrum of the $S_2^{\bullet\bullet}\cdot Q_A$ state characterized by the multiline (*24*) and $g = 4.1$ (*25*) components. Figure 1b shows the spectrum recorded after flash illumination at 190 K followed by rapid heating to −10 °C. Advancement to S_3 has been achieved in a fraction of centers, as indicated by the characteristic S_3 state $g = 10$ signal (*26*) at the expense of the S_2 state signals. Clearly, illumination of the $S_2\cdots Q_A$ state at 190 K produces an intermediate that advances to S_3 at elevated temperatures. This is a low-efficiency process (the competing oxidation of cyt b_{559} can also be noted in Figure 1b), the effect of a single cycle being ca. 6−7%. Hence, it had to be repeated

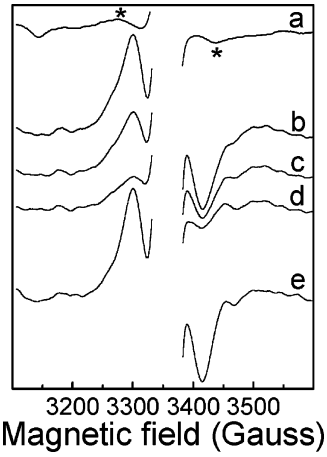

FIGURE 2: Trapping of a new metalloradical species: (a) flash illumination of S_2 at 10 K without prior treatment, (b) flash illumination of the S_2 state at 190 K followed by rapid (1−2 s) cooling to 77 K and from there into the EPR cryostat at 10 K, (c) subsequent incubation at 10 K for 4 min, (d) additional incubation at 10 K for a total of 15 min, and (e) subsequent flash illumination at 10 K. The spectrum of S_2 prior to additional illuminations was subtracted from all traces. EPR conditions were as described in the legend of Figure 1.

several times to obtain the observed 35% decrease in the amount of S_2 in Figure 1b. Results similar to those in Figure 1 but with a somewhat lower efficiency in the S_2 to S_3 conversion were obtained by flash illumination at 150 K and rapid heating to −10 °C.

These experiments show that an intermediate of the S_2 to S_3 transition is formed at temperatures much lower than the threshold for the S_2 to S_3 transition. In an effort to trap this intermediate, the sample in the S_2 state, following flash illumination at 190 K, was cooled quickly to 10 K. Figure 2b shows that a 116 G wide signal was trapped, which in 4 min decayed by ∼40% (Figure 2c) and in 15 min by ∼80% (Figure 2d). The signal could be re-induced after its decay by illumination at 10 K (Figure 2e). By comparison, illumination of the initial S_2 state at 10 K (Figure 2a) yields nothing more than a weak contribution (marked by the asterisks) resulting probably from a minority of centers that are in S_0 (*7*). Spectra similar to the one shown in Figure 2e could be repeatedly induced following the decay of the signal and subsequent illumination at 10 K. Preliminary experiments showed that the new signal, like those of other metalloradical signals (*5*−*10*, *15*−*20*, *27*), does not saturate easily ($P_{1/2}$ > 20 mW at 10 K).

To test that the metalloradical signal trapped at liquid helium temperatures represents a true S_2 to S_3 transition intermediate, a sample in the $S_2\cdots Q_A$ state (Figure 3a) was flash-illuminated at 190 K and rapidly cooled to 10 K as in Figure 2b. The sample was then given an additional flash at 10 K as in Figure 2e (i.e., after incubation for 15 min at 10 K) and heated rapidly to −10 °C. The whole cycle was repeated 10 times to account for recombination and other losses, and the final spectrum (Figure 3b) was recorded. A decrease of ∼25% in the S_2 signals can be observed, accompanied by the evolution of the S_3 spectrum at $g = 10$.

The experiment in Figure 2 was repeated by illumination at temperatures lower than 190 K (Figure 4). A sizable signal was obtained by illumination at 150 K, while the signal declined at 120 K and became very small when the flash

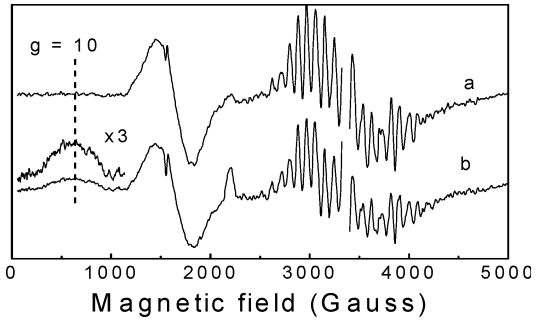

FIGURE 3: Metalloradical signal of the untreated S_2 state advances to S_3 at elevated temperatures. Spectra are differences from the S_1 state. (a) Spectrum of the $S_2\cdots Q_A$ state. (b) Subsequent application of the following cycle 10 times: flash illumination at 190 K, followed by rapid cooling to 10 K and incubation for 15 min in the cryostat, followed by flash illumination at 10 K, and immediate transfer and incubation at −10 °C for 1 min. EPR conditions were as described in the legend of Figure 1.

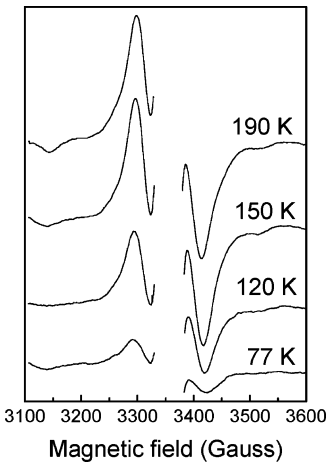

FIGURE 4: Dependence of the size of the S_2 metalloradical signal on the temperature of pre-illumination. The sample was preflashed at the indicated temperature and rapidly transferred to the EPR cryostat at 10 K. Another flash was administered at 10 K, and the spectrum was collected immediately afterward. The difference spectrum that is shown was obtained by subtraction of the spectrum collected approximately 20 min after flash illumination at 10 K. EPR conditions were as described in the legend of Figure 1.

was given at 77 K. The spectra shown in Figure 4 are those produced by illumination at 10 K following the decay of the signal at the same temperature. In all cases, there was a good correlation between the size of the signal trapped immediately after the elevated temperature illumination and the size of the signal re-induced at 10 K. The only difference was that the former spectrum had somewhat broader features.

The recovered S_2 conformation following decay of the radical signal at 10 K has an EPR spectrum similar within experimental uncertainty to that of the high-temperature S_2 conformation. Formation of the radical signal is accompanied by a decrease in the size of the multiline signal. This is visible in the superposition of the multiline spectra prior to (black) and after illumination at 10 K (red) in Figure 5A, but it is more clearly depicted by the comparison of the difference of the low-field part of the multiline spectra (blue trace) with the scaled down (factor of 0.2) pre-illumination multiline spectrum (black trace) in Figure 5B. Besides the notable size of the difference spectrum (indicating a ca. 20% decrease in multiline intensity upon formation of the radical), small but

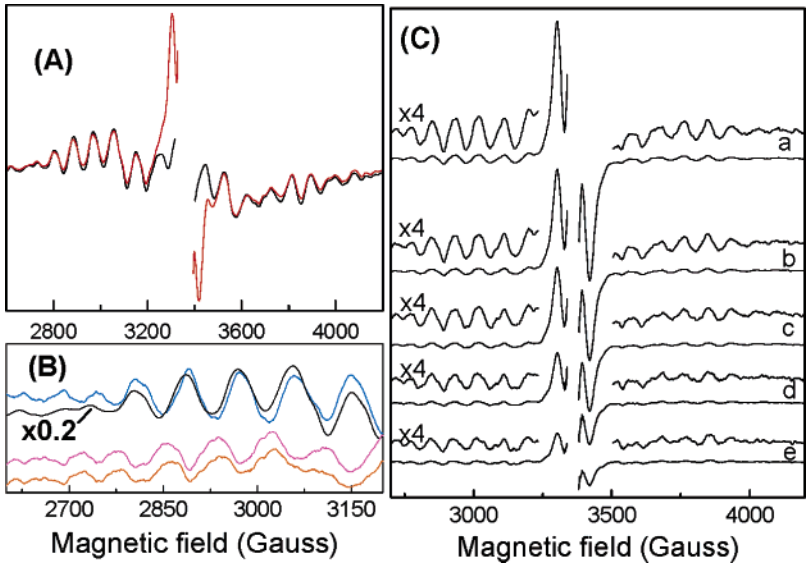

FIGURE 5: Reversible changes in the S_2 state multiline signal during formation and decay of the metalloradical signal produced as in Figure 2e. (A) Superposition of the multiline spectra (following subtraction of the S_1 background spectrum) prior to (black) and after (red trace) flash illumination at 10 K. (B) Comparisons of the low-field part of the multiline spectra. The blue trace is the difference (black trace minus red trace) of the spectra in panel A compared with 20% of the pre-illuminated multiline spectrum; magenta and orange traces show the subtraction of 90 and 85%, respectively, of the pre-illuminated spectrum from the post-illuminated one. (C) Following the flash at 10 K, spectra were collected at (a) 15, (b) 90, (c) 170, (d) 330, and (e) 560 s. From the spectra, the full pre-illumination spectrum of the S_2 state was subtracted. EPR conditions were as described in the legend of Figure 1. The scan time of each spectrum is 45 s. The *y*-scale in each panel has independent units.

reproducible changes in the multiline features can be observed, implying that the decrease in the size of the multiline signal is due to modification rather than elimination. Figure 5C shows that the decrease in the multiline signal intensity is eliminated in parallel with the decay (by charge recombination) of the radical signal. It is likely that the changes observed in the multiline signal are due to a magnetic interaction of the radical with the Mn. To obtain a rough estimate of the fraction of centers contributing to the radical formation, the area of the integrated radical spectrum (region from 3200 to 3500 in spectrum a of Figure 5C) was compared with the area of the integrated pre-illumination multiline spectrum. A fraction of 10−12% was estimated. The magenta and orange traces in Figure 5B show the result of subtraction of 90 and 85%, respectively, of the pre-illumination spectrum from the post-illumination one. A shifted (almost out of phase) multiline signal appears which presumably accompanies the radical species. The situation is strongly reminiscent of the interaction of Tyr $Z^{\bullet}$ with Mn in acetate-treated samples (*28*), but this analysis is clearly preliminary. No changes could be detected in the $g = 4.1$ signal during radical formation.

Trapping of a Metalloradical Signal in the S_2 State in the Presence of Methanol. Addition of few percent (v/v) methanol in PSII samples does not inhibit O_2 evolution (*29*) but has several effects on the EPR signals. It produces a uniform population of S_2 exhibiting only the multiline signal (*30*), eliminates the S_3 EPR spectrum (*26*), allows observation of the S_0 spectrum (*31*, *32*), and eliminates the NIR sensitivity of the S_2 and S_3 states (*33*, *34*); the split signal in S_0 trapped at liquid helium temperatures becomes broader (*7*, *27*), while the split signal in S_1 is eliminated (*5*). The experiment of Figure 6 shows that this kind of samples produces a split signal upon flash illumination of the $S_2\cdots Q_A$ state at 10 K. Figure 6b shows this signal as a difference spectrum. It has a typical split pattern with a width of 160 G. Figure 6a shows

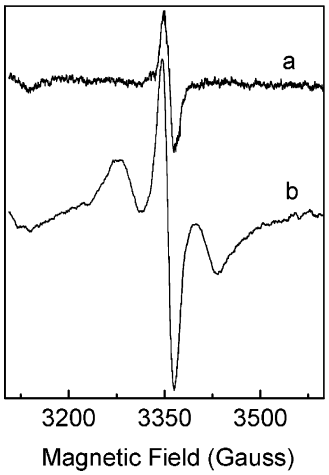

FIGURE 6: Trapping of a metalloradical signal in the S_2 state of samples containing 5% (v/v) methanol. Flash illumination at 10 K of (a) a sample poised in the $S_2\cdots Q_A^-$ state and (b) a sample prepared in the $S_2\cdots Q_A$ state. The background spectra obtained after dark adaptation for 15 min at 10 K were subtracted. EPR conditions: microwave frequency of 9.407 GHz, temperature of 10 K, modulation amplitude of 12.5 G, and microwave power of 115 mW.

that no split signal is produced in the $S_2\cdots Q_A^-$ state, implying that the signal in Figure 6b is the product of charge separation. Preliminary investigations of the microwave power saturation of the signal indicated that at 10 K the $P_{1/2}$ is greater than 100 mW. Similar spectra are obtained under the EPR conditions of Figure 1, except that the nonidentified free radical contributions at $g = 2.0$ become less saturated.

Production of the metalloradical signal in S_2 is accompanied by a decrease in the size of the multiline signal, as shown in the difference spectra of Figure 7. Within the signal-to-noise range, the changes disappear in parallel with the decay of the split signal. A rough quantitation similar to the one in relation to Figure 5 indicated that the radical signal

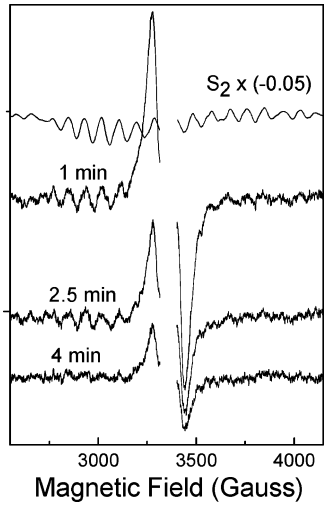

FIGURE 7: Reversible changes in the S_2 state multiline signal in samples containing 5% (v/v) MeOH, during formation and decay of the metalloradical signal produced as in Figure 6b. Recording of the spectra started at the indicated times after flash illumination at 10 K. The background spectra obtained after dark adaptation at 10 K were subtracted from all traces except the top trace which is the S_2 multiline signal multiplied by −0.05 for comparison. EPR conditions: microwave frequency of 9.407 GHz, temperature of 10 K, modulation amplitude of 25 G, microwave power of 115 mW, and sweep time of 50 s.

represents 4−6% of the multiline signal-producing centers. The radical signal decays at 10 K with a $t_{1/2}$ of ∼80 s (experiments in progress).

DISCUSSION

Assignment of the Metalloradical Signals to $S_2Y_Z^\bullet$. In an earlier paper, we summarized the observations that favor the assignment of the various metalloradical signals to Tyr $Z^\bullet$ (*10*). (i) The transients can advance to the next S state at elevated temperatures, and this is compatible with the fact that Tyr $Z^\bullet$ is the natural oxidant of the Mn cluster. (ii) The EPR signals are reminiscent of the signals obtained in preparations inhibited in the S_2 to S_3 step by acetate treatment or calcium depletion, attributed by most authors to an $S_2Y_Z^\bullet$ intermediate. (iii) The small distance from Tyr Z to the Mn cluster is compatible with the observed magnetic broadening and the fast relaxation of the EPR signals, as well as the fact that the signals vary in shape with the oxidation state (and therefore the spin state) of the Mn cluster. (iv) No other known electron donors exhibit any of the properties mentioned above. Our results provide an additional observation concerning the S_2 to S_3 intermediates. (v) The S_2 multiline signal is reversibly modified parallel with the formation and/or decay of the metalloradical signals. This is reminiscent of the changes observed in Ca^{2+}-depleted and acetate-treated PSII preparations during formation of the $S_2Y_z^\bullet$ intermediate (*16*, *28*). We will therefore assign the present signals to Tyr $Z^\bullet$ ($S = {}^1/_2$) magnetically interacting with the multiline ($S = {}^1/_2$) configuration of S_2 (it is unclear at present whether an intermediate corresponding to the $g = 4.1$ configuration of S_2 can be trapped).

Temperature Constraints. An elementary model that can explain the constraints for Tyr Z oxidation in S_2 (untreated samples) compared with the unconstrained oxidation in S_0 and S_1 is described in Scheme 1. It is assumed that the

Scheme 1: Elementary Proposal for the Oxidation of Tyr Z in the S_2 State[a]

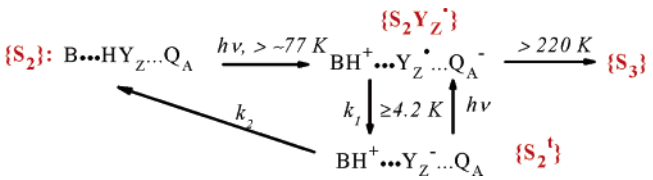

[a] The deprotonation of Tyr Z during its oxidation requires temperatures higher than 77 K. Reprotonation of Tyr Z^- is not possible at liquid helium temperatures. S_2^t is a trapped S_2 state configuration in which the functional redox couple is Tyr $Z^\bullet$/Tyr Z^-. See the text for more elaborate possibilities.

positive charge on the Mn cluster in S_2 weakens the hydrogen bond of Tyr Z with its base partner B (*10*). Accordingly, a higher temperature is required for the activation of proton motion during oxidation of Tyr Z in S_2 in comparison with that of the lower S states. The fact that the intermediate can be repeatedly formed by illumination at 10 K indicates that the proton does not return to Tyr Z following its reduction (presumably by Q_A^-), and therefore, the functional redox couple is probably Tyr $Z^\bullet$/Tyr Z^-.

An extension of Scheme 1 would consider secondary proton transfer or molecular motions that could be activated above 77 K (see, for example, the elegant treatment of the stable tyrD radical in ref *35*). McEvoy and Brudvig (*36*) have proposed that His 190 protonation during Tyr Z oxidation triggers the deprotonation of CP43-Arg357, and this relaxes the excess positive charge in the vicinity of His 190. Alternatively, D1-Asn 298, which lies close to His 190 (*13*, *14*), may act as a secondary H^+ acceptor. The fact that changes can occur at 77 K, resulting in the removal of barriers for Tyr Z oxidation at 4.2 K, was alternatively shown by the one-electron reduction of the S_3 state by Q_A^- at 77 K. In this process, the S_2' state was formed, in which Tyr Z was readily oxidized at 4.2 K (*9*, *10*).

The comparison with the MeOH-containing samples is less straightforward. MeOH changes the coordination of the Mn cluster at a suggested position (see below) that may affect the Tyr Z−His 190 coupling. Also, the high concentrations of MeOH that were used may have global nonspecific effects. The effects of MeOH on the S states should be evaluated independently in future studies.

A Molecular Model. It would be instructive to examine these results in the context of the molecular model of Figure 8, which extends our earlier suggestion (*10*) and is structurally supported by the most recent crystallographic results (*14*). Essential parts of the model besides the Mn cluster are Glu 189, which binds to ^{1}Mn and the Ca^{2+} cofactor, and His 190, which functions as the base partner of Tyr Z. It has been suggested that during the S_1 to S_2 transition ^{2}Mn(III) is oxidized to ^{2}Mn(IV) (*14*, *37*). We will assume that ^{1}Mn is in the +3 oxidation state in S_1 and S_2 (and S_3; see below), while the other two Mn ions are in the +4 oxidation state (see refs *1* and *2* for critical consideration of alternative valence state assignments; see also ref *14*). In our earlier model (*10*) showing schematically only the Mn adjacent to Glu 189, we assumed oxidation of that ion during the S_1 to S_2 step. The specific valence assignment in S_2 presented here, ^{1}Mn(III)−^{2}Mn(IV)−^{3,4}Mn(IV), can explain a number of observations, as will be discussed below.

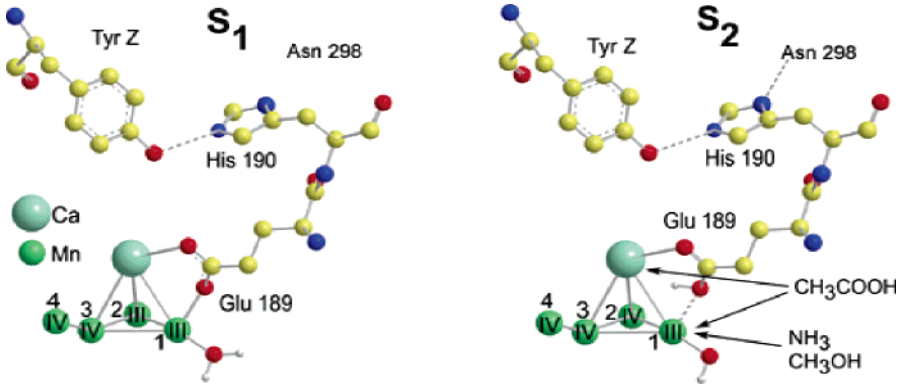

FIGURE 8: Molecular model extending our earlier suggestion (*10*), structurally supported by the most recent crystallographic results (*14*). During the S_1 to S_2 transition, ^{2}Mn(III) is oxidized to ^{2}Mn(IV), and this is accompanied by a proton movement from water bound to ^{1}Mn(III) to Glu 189. This weakens the bond of Glu 189 with ^{1}Mn(III). The special environment of ^{1}Mn(III) is preserved in S_3 and is responsible for the NIR sensitivity of the Mn cluster. ^{1}Mn(III) is also a likely binding site of small exogenous molecules. Asp 298, which according to ref *14* is within hydrogen bonding distance of His 190, is suggested to act as a secondary proton acceptor during oxidation of Tyr Z.

It was suggested in ref *10* that the oxidation of Mn during the S_1 to S_2 step is compensated by proton transfer from the water ligand of ^{1}Mn to Glu 189. Such a transfer should in principle be able to be detected by FTIR spectroscopy. S_2/S_1 difference FTIR bands associated with Glu 189 have been assigned recently by comparison with the Glu 189 Gln mutant in the 1600−1300 cm^{-1} region (*38*), the region assigned to stretching modes from the putative carboxylate ligands to Mn. In our model, Glu 189 is a bridging ligand to Ca^{2+} and to ^{1}Mn(III) in both S_1 and S_2; therefore, changes accompanying the protonation of Glu 189 (this only weakens and does not disrupt the bond to ^{1}Mn) should appear in the above regions rather than in the region of 1790−1710 cm^{-1} where modes from protonated free carboxylates are expected to appear. To the best of our knowledge of the complex FTIR spectra, the region of 1600−1300 cm^{-1} is too congested to identify changes associated with the suggested protonation of Glu 189 in Figure 8. The mere fact, however, that changes are observed in the carboxylate stretching modes during the S_1 to S_2 transition is consistent with the suggested weakening of the Glu 189−Mn bond. An indication of these ambiguities in the interpretation of the FTIR spectra is that the evaluation of the FTIR results suggests bidentate binding to a single Mn ion, while the recent crystallographic analysis indicates bridging ligation.

The protonation of Glu 189 during the S_1 to S_2 step has several consequences. The presence of the excess positive charge in the vicinity of ^{1}Mn(III) may be a key factor in increasing the redox potential of this particular ion and preventing its early oxidation. This may be mechanistically important particularly if the water bound to this Mn is substrate water. The protonation of Glu 189 modifies the proton accepting ability of His 190 (change in the relative p*K* and/or the distance from Tyr Z) and imposes temperature barriers to the activation of the proton transfer from Tyr Z to His 190 during oxidation of the former. It may also increase the operating redox potential of Tyr Z in the higher S state transitions.

The NIR Sensitivity Is Attributed to ^{1}Mn(III). ^{1}Mn(III) has a unique environment in S_2. The Jahn−Teller distortion in this case may well be in the NIR frequency range, and this makes this Mn an excellent candidate for the NIR sensitivity of the Mn cluster observed in only S_2 and S_3 (*6*, *34*, *39*). The action spectrum of the NIR effect is very similar in both states (*40*), and this strongly suggests that the special ^{1}Mn(III) environment is preserved in S_3.

Multiline and $g = 4.1$ Conformations of the S_2 State. The ^{1}Mn(III)−^{2}Mn(IV)−^{3,4}Mn(IV) conformation gives rise to the multiline EPR signal in S_2. The $g = 4.1$ signal could correspond to the ^{1}Mn(IV)−^{2}Mn(III)−^{3,4}Mn(IV) conformation which for some reason is energetically preferred in a minority of centers. It is interesting that the $g = 4.1$ conformation is not sensitive to NIR excitation. On the other hand, NIR excitation of the multiline conformation gives rise to the $g = 4.1$ conformation; i.e., it induces electron transfer from ^{1}Mn(III) to ^{2}Mn(IV).

Tentative Suggestions about the Binding of Exogenous Molecules; D1-Glu 189 Mutants. The protonation of Glu 189 in S_2 should weaken its bond with ^{1}Mn. Hence, ^{1}Mn(III) is a likely site for the binding of small exogenous molecules in S_2 such as MeOH and NH_3. Both MeOH [*28*, *29*, *42*; see also ref *43* for suggested binding to Mn(III)] and NH_3 (*44*) bind with greater affinity to the S_2 state, and they both remain bound in the S_3 state (*26*, *34*, *45*), which according to the suggestions presented here preserves the special environment of ^{1}Mn(III). Recent MeOH/NH_3 competition studies would be most readily interpreted as competitive binding to the same side (*46*, *47*; but see ref *41*). Presumably, the distortion of the special environment of ^{1}Mn(III) by the MeOH and NH_3 binding eliminates the NIR sensitivity in both S_2 and S_3 as observed experimentally (ref *45* for NH_3 and refs *33* and *34* for MeOH). It is notable on the other hand that perturbation of the Ca^{2+} binding site by Ca^{2+} removal (and/or substitution with Sr^{2+}) results in preparations that retain their NIR sensitivity (*39*, *40*, *45*). In this case, the connection between Glu 189 and ^{1}Mn is presumably not distorted.

Acetate (*17*−*20*) is suggested to replace fully Glu 189; the ability to store the proton on the S_1 to S_2 transition is presumably lost, and this transition requires elevated temperatures to support proton movement over a longer distance or to the aqueous phase like all other transitions. Acetate with its negative charge lowers the redox potential of ^{1}Mn and stabilizes the ^{1}Mn(IV)−^{2}Mn(III)−^{3,4}Mn(IV) configuration, characterized by the experimentally observed $g = 4.1$ EPR spectrum. The NIR sensitivity is also lost (our unpublished observations). Formation of the $S_2Y_Z^{\bullet}$(acetate) species

has a much higher temperature of activation (>250 K) (*17*−*20*) compared with the untreated system (>77 K) (this work). Presumably, the binding of acetate distorts the Tyr Z−His 190 coupling, imposing strict thermal barriers to the deprotonation of Tyr Z upon its oxidation. The other end of the proposed binding of acetate, Ca^{2+}, could interfere with chloride binding (*48*). Finally, the extended stability of $S_2Y_Z^{\bullet}$ with acetate suggests that the E_m of Tyr Z is quite low; this can be attributed to the excess negative charge (Glu 189 and acetate) on the cluster.

Mutation work on D1-Glu 189 (*49*) shows that of 17 mutants that were examined only five (Gln, Lys, Arg, Leu, and Ile) sustain O_2 evolution (at decreased levels, 40−80% of the wild type). Twelve mutants are incapable of O_2 evolution, but some of them give split signals by illumination at 273 K (*49*), a behavior reminiscent of the acetate effect [some of the mutants may ligate ^{1}Mn via their backbone carbonyl group (*38*)]. The least drastic of the mutations, Glu 189 to Gln, supports formation of the multiline signal at 195 K. It is possible that Gln can satisfactorily replace Glu 189 (see also ref *38*) and even act as a low-temperature proton acceptor. It is not easy, however, to explain in simple terms the absence of appreciable changes in the rates of electron transfer from Tyr Z to P_{680}^+ and from the Mn cluster to Tyr $Z^{\bullet}$, during the S_1 to S_2 and S_2 to S_3 transitions, in the Glu 189 Gln, Glu 189 Lys, and Glu 189 Arg mutants (*50*). It has been suggested that a cluster of acid−base groups around D1-Glu 189 compensates for the alteration of charge in the mutants (*50*). An example of the compensating changes that occur is the recent observation that the redox potential of the S_2/S_1 couple is lowered in the Glu189Gln mutant (*38*). A comparison of the low-temperature barriers for Tyr Z oxidation (and reduction) in various S states of some of these mutants might be particularly enlightening.

ACKNOWLEDGMENT

We thank Dr. Y. Sanakis for useful discussions.

REFERENCES

1. Goussias, C., Boussac, A., and Rutherford, A. W. (2002) Photosystem II and photosynthetic oxidation of water: An overview, *Philos. Trans. R. Soc. London, Ser. B 357*, 1369−1381.
2. Carrell, T. G., Tyryskin, A. M., and Dismukes, G. C. (2002) An evaluation of structural models for the photosynthetic water-oxidizing complex derived from spectroscopic and X-ray diffraction signatures, *J. Biol. Inorg. Chem. 7*, 2−22.
3. Brudvig, G. W., Casey, J. L., and Sauer, K. (1983) The effect of temperature on the formation and decay of the multiline EPR signal species associated with photosynthetic oxygen evolution, *Biochim. Biophys. Acta 723*, 366−371.
4. Styring, S., and Rutherford, A. W. (1988) Deactivation kinetics and temperature dependence of the S-state transitions in the oxygen-evolving system of photosystem II measured by EPR spectroscopy, *Biochim. Biophys. Acta 933*, 378−387.
5. Nugent, J. H. A., Muhiuddin, I. P., and Evans, M. C. W. (2002) Electron transfer from the water oxidizing complex at cryogenic temperatures: The S_1 to S_2 step, *Biochemistry 41*, 4117−4126.
6. Koulougliotis, D., Shen, J. R., Ioannidis, N., and Petrouleas, V. (2003) Near-IR irradiation of the S_2 state of the water oxidizing complex of photosystem II at liquid helium temperatures produces the metalloradical intermediate attributed to $S_1Y_Z^{\bullet}$, *Biochemistry 42*, 3045−3053.
7. Zhang, C. X., and Styring, S. (2003) Formation of split electron paramagnetic resonance signals in photosystem II suggests that tyrosine Z can be photooxidized at 5 K in the S_0 and S_1 states of the oxygen-evolving complex, *Biochemistry 42*, 8066−8076.
8. Zhang, C. X., Boussac, A., and Rutherford, A. W. (2004) Low-Temperature Electron Transfer in Photosystem II: A Tyrosyl Radical and Semiquinone Charge Pair, *Biochemistry 43*, 13787−13795.
9. Ioannidis, N., Nugent, J. H. A., and Petrouleas, V. (2002) Intermediates of the S_3 State of the Oxygen-Evolving Complex of Photosystem II, *Biochemistry 41*, 9589−9600.
10. Petrouleas, V., Koulougliotis, D., and Ioannidis, N. (2005) Trapping of Metalloradical Intermediates of the S-States at Liquid Helium Temperatures. Overview of the Phenomenology and Mechanistic Implications, *Biochemistry 44*, 6723−6728.
11. Diner, B. A. (2001) Amino acid residues involved in the coordination and assembly of the manganese cluster of photosystem II. Proton-coupled electron transport of the redox-active tyrosines and its relationship to water oxidation, *Biochim. Biophys. Acta 1503*, 147−163.
12. Kamiya, N., and Shen, J. R. (2003) Crystal structure of oxygen-evolving photosystem II from *Thermosynechococcus vulcanus* at 3.7-Å resolution, *Proc. Natl. Acad. Sci. U.S.A. 100*, 98−103.
13. Ferreira, K. N., Iverson, T. M., Maghlaoui, K., Barber, J., and Iwata, S. (2004) Architecture of the photosynthetic oxygen-evolving center, *Science 303*, 1831−1838.
14. Loll, B., Kern, J., Saenger, W., Zouni, A., and Biesiadka, J. (2005) Towards complete cofactor arrangement in the 3.0 Å resolution structure of photosystem II, *Nat. Lett. 438*, 1040−1044.
15. Geijer, P., Morvaridi, F., and Styring, S. (2001) The S_3-state of the oxygen-evolving complex in photosystem II is converted to the $S_2Y_Z^{\bullet}$ at alkaline pH, *Biochemistry 40*, 10881−10891.
16. Boussac, A., Zimmermann, J. L., and Rutherford, A. W. (1989) EPR signals from modified charge accumulation states of the oxygen-evolving enzyme in calcium-deficient photosystem II, *Biochemistry 28*, 8984−8989.
17. MacLachlan, D. J., and Nugent, J. H. A. (1993) Investigation of the S_3 Electron Paramagnetic Resonance Signal from the Oxygen-Evolving Complex of Photosystem 2: Effect of Inhibition of Oxygen Evolution by Acetate, *Biochemistry 32*, 9772−9780.
18. Lakshmi, K. V., Eaton, S. S., Eaton, G. R., Frank, H. A., and Brudvig, G. W. (1998) Analysis of Dipolar and Exchange Interactions between Manganese and Tyrosine Z in the $S_2Y_Z^{\bullet}$ State of Acetate-Inhibited Photosystem II via EPR Spectral Simulations at X- and Q-Bands, *J. Phys. Chem. B 102*, 8327−8335.
19. Peloquin, J. M., Campbell, K. A., and Britt, R. D. (1998) ^{55}Mn Pulsed ENDOR Demonstrates That the Photosystem II "Split" EPR Signal Arises from a Magnetically-Coupled Mangano-Tyrosyl Complex, *J. Am. Chem. Soc. 120*, 6840−6841.
20. Dorlet, P., Di Valentin, M., Babcock, G. T., and McCracken, J. L. (1998) Interaction of $Y_Z^{\bullet}$ with Its Environment in Acetate-Treated Photosystem II Membranes and Reaction Center Cores, *J. Phys. Chem. B 102*, 8239−8247.
21. Mino, H., and Itoh, S. (2005) The origin of split EPR signals in the Ca^{2+}-depleted photosystem II, *Photosynth. Res. 84*, 333−337.
22. Berthold, D. A., Babcock, G. T., and Yocum, C. F. (1981) A highly resolved, oxygen-evolving photosystem II preparation from spinach thylakoid membranes, *FEBS Lett. 134*, 231−234.
23. Petrouleas, V., and Diner, B. A. (1987) Light-induced oxidation of the acceptor-side Fe(II) of photosystem II by exogenous quinones acting through the Q_B binding site. I. Quinones, kinetics and pH dependence, *Biochim. Biophys. Acta 893*, 126−137.
24. Dismukes, G. C., and Siderer, Y. (1981) Intermediates of a polynuclear center involved in photosynthetic oxidation of water, *Proc. Natl. Acad. Sci. U.S.A. 78*, 274−278.
25. Casey, J. L., and Sauer, K. (1984) EPR detection of a cryogenically photogenerated Intermediate in Photosynthetic Oxygen Evolution, *Biochim. Biophys. Acta 767*, 21−28.
26. Matsukawa, T., Mino, H., Yoneda, D., and Kawamori, A. (1999) Dual-Mode EPR Study of New Signals from the S_3-State of Oxygen-Evolving Complex in Photosystem II, *Biochemistry 38*, 4072−4077.
27. Nugent, J. H. A., Muhiuddin, I. P., and Evans, M. C. W. (2003) Effects of Hydroxylamine on Photosystem II: Reinvestigation of Electron Paramagnetic Resonance Characteristics Reveals Possible S state Intermediates, *Biochemistry 42*, 5500−5507.
28. Szalai, V., Kühne, H., Lakshmi, K. V., and Brudvig, G. W. (1998) Characterization of the Interaction between Manganese and Tyrosine Z in Acetate-Inhibited Photosystem II, *Biochemistry 37*, 13594−13603.
29. Force, A., Randall, D. W., Lorigan, G. A., Clemens, K. L., and Britt, R. (1998) ESEEM Studies of Alcohol Binding to the

Manganese Cluster of the Oxygen Evolving Complex of Photosystem II, *J. Am. Chem. Soc. 120*, 13321−13333.
30. Pace, R. J., Smith, P., Bramley, R., and Stehlik, D. (1991) EPR Saturation and Temperature-dependence studies on signals from the Oxygen-Evolving center of Photosystem II, *Biochim. Biophys. Acta 1058*, 161−170.
31. Messinger, J., Nugent, J. H. A., and Michael, E. (1997) Detection of an EPR Multiline Signal for the S_0* state in Photosystem II, *Biochemistry 36*, 11055−11060.
32. Ahrling, K. A., Peterson, S., and Styring, S. (1997) An Oscillating Manganese Electron Paramagnetic Resonance Signal from the S_0 State of the Oxygen Evolving Complex in Photosystem II, *Biochemistry 36*, 13148−13152.
33. Boussac, A., Deligiannakis, Y., and Rutherford, A. W. (1998) Effects of Methanol on the Mn_4-cluster of Photosystem II, in *Photosynthesis: Mechanism and Effects* (Garab, G., Ed.) Vol. II, pp 1233−1240, Kluwer Academic Publishers, Dordrecht, The Netherlands.
34. Ioannidis, N., and Petrouleas, V. (2000) Electron Paramagnetic Resonance Signals from the S_3 State of the Oxygen-Evolving Complex. A Broadened Radical Signal Induced by Low-Temperature Near-Infrared Light Illumination, *Biochemistry 39*, 5246−5254.
35. Faller, P., Goussias, C., Rutherford, A. W., and Un, S. (2003) Resolving intermediates in biological proton−coupled electron transfer: A tyrosyl radical prior to proton movement, *Proc. Natl. Acad. Sci. U.S.A. 100*, 8732−8735.
36. McEvoy, J. P., and Brudvig, G. W. (2004) Structure-based mechanism of photosynthetic water oxidation, *Phys. Chem. Chem. Phys. 6*, 4754−4763.
37. Chu, H.-A., Hillier, W., and Debus, R. J. (2004) Evidence that the C-Terminus of the D1 Polypeptide of Photosystem II is Ligated to the Manganese Ion that Undergoes Oxidation During the S1 to S2 Transition: An Isotope-Edited FTIR Study, *Biochemistry 43*, 3152−3166.
38. Kimura, Y., Mizusawa, N., Ishii, A., Shigeaki Nakazawa, S., and Taka-aki Ono, T. (2005) Changes in Structural and Functional Properties of Oxygen-evolving Complex Induced by Replacement of D1-Glutamate 189 with Glutamine in Photosystem II. Ligation of Glutamate 189 Carboxylate to the Manganese Cluster, *J. Biol. Chem. 280*, 37895−37900.
39. Boussac, A., Girerd, J. J., and Rutherford, A. W. (1996) Conversion of the Spin State of the Manganese Complex in Photosystem II Induced by Near-Infrared Light, *Biochemistry 35*, 6984−6989.
40. Boussac, A., Sugiura, M., Kirilovsky, D., and Rutherford, A. W. (2005) Near-infrared-induced Transitions in the Manganese Cluster of Photosystem II: Action Spectra for the S2 and S3 Redox States, *Plant Cell Physiol. 46* (6), 837−842.
41. Britt, R. D., Campbell, K. A., Peloquin, J. M., Gilchrist, M. L., Aznar, C. P., Dicus, M. M., Robblee, J., and Messinger, J. (2004) Recent pulsed EPR studies of the Photosystem II oxygen-evolving complex: Implications as to water oxidation mechanisms, *Biochim. Biophys. Acta 1655*, 158−171.
42. Deak, Z., Peterson, S., Geijer, P., Ahrling, K. A., and Styring, S. (1999) Methanol modification of the electron paramagnetic resonance from the S_0 and S_2 states of the water-oxidizing complex of photosystem II, *Biochim. Biophys. Acta 1412*, 240−249.
43. Arling, K. A., Evans, M. C. W., Nugent, J. H. A., and Pace, R. J. (2004) The two forms of the S_2 state multiline signal in photosystem II: Effect of methanol and ethanol, *Biochim. Biophys. Acta 1656*, 66−77.
44. Beck, W. F., de Paula, J. C., and Brudvig, G. W. (1986) Ammonia binds to the manganese site of the O_2-evolving complex of photosystem II in the S_2 state, *J. Am. Chem. Soc. 108*, 4018−4022.
45. Boussac, A., Sugiura, M., Inoue, Y., and Rutherford, A. W. (2000) EPR Study of the Oxygen Evolving Complex in His-Tagged Photosystem II from the Cyanobacterium *Synechococcus elongatus*, *Biochemistry 39*, 13788−13799.
46. Evans, M. C. W., Ball, R. J., and Nugent, J. H. A. (2005) Ammonia displaces methanol bound to the water oxidizing complex of photosystem II in the S_2 state, *FEBS Lett. 579*, 3081−3084.
47. Fang, C.-H., Chiang, K.-A., Hung, C.-H., Chang, K., Ke, S.-C., and Chu, H.-A. (2005) Effects of ethylene glycol and methanol on ammonia-induced structural changes of the oxygen-evolving complex in photosystem II, *Biochemistry 44*, 9758−97654.
48. Kühne, H., Szalai, V., and Brudvig, G. W. (1999) Competitive Binding of Acetate and Chloride in Photosystem II, *Biochemistry 38*, 6604−6613.
49. Debus, R. J., Campbell, K. A., Pham, D. P., Hays, A.-M. A., and Britt, R. D. (2000) Glutamate 189 of the D1 Polypeptide Modulates the Magnetic and Redox Properties of the Manganese Cluster and Tyrosine Y_Z in Photosystem II, *Biochemistry 39*, 6275−6287.
50. Clausen, J., Winkler, S., Hays, A.-M. A., Hundelt, M., Debus, R. J., and Junge, W. (2001) Photosynthetic water oxidation in *Synechocystis* sp. PCC6803: Mutations D1-E189K, R and Q are without influence on electron transfer at the donor side of photosystem II, *Biochim. Biophys. Acta 1506*, 224−235.

BI060520S